

HACD: Hand-Aware Conditional Diffusion for Monocular Hand-Held Object Reconstruction

Bowen Fu^{1,2*}, Yan Di^{2*}, Chenyangguang Zhang¹, Gu Wang¹, Ziqin Huang¹, Zhiying Leng²,
Fabian Manhardt³, Xiangyang Ji¹ and Federico Tombari^{2,3}

¹Tsinghua University ²Technical University of Munich ³Google

fbw19@mails.tsinghua.edu.cn

Abstract

Reconstructing hand-held objects from a single RGB image without known 3D object templates, category prior, or depth information is a vital yet challenging problem in computer vision. In contrast to prior works that utilize deterministic modeling paradigms, which make it hard to account for the uncertainties introduced by hand- and self-occlusion, we employ a probabilistic point cloud denoising diffusion model to tackle the above challenge. In this work, we present **Hand-Aware Conditional Diffusion** for monocular hand-held object reconstruction (HACD), modeling the hand-object interaction in two aspects. First, we introduce hand-aware conditioning to model hand-object interaction from both semantic and geometric perspectives. Specifically, a unified hand-object semantic embedding compensates for the 2D local feature deficiency induced by hand occlusion, and a hand articulation embedding further encodes the relationship between object vertices and hand joints. Second, we propose a hand-constrained centroid fixing scheme, which utilizes hand vertices priors to restrict the centroid deviation of partially denoised point cloud during diffusion and reverse process. Removing the centroid bias interference allows the diffusion models to focus on the reconstruction of shape, thus enhancing the stability and precision of local feature projection. Experiments on the synthetic ObMan dataset and two real-world datasets, HO3D and MOW, demonstrate our approach surpasses all existing methods by a large margin.

1. Introduction

Modelling hand-object interactions has a wide range of applications across various domains, including AR/VR [38, 54, 55] and robotics [24, 72, 75]. Significant progress has been made in this task [4, 38, 72], in which single-view

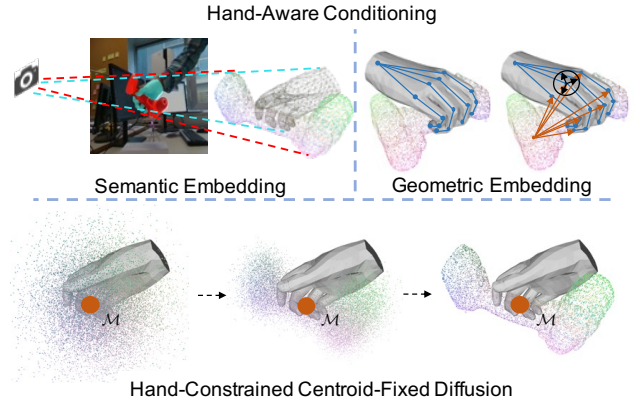


Figure 1. We present hand-aware conditioning, utilizing both semantic and geometric embeddings to model hand-object interaction. We further propose hand-constrained centroid-fixed diffusion, where the centroid of the partially denoised point cloud at each step is constrained by the hand vertices and kept fixed throughout the whole diffusion and the reverse process.

hand-held object reconstruction draws particularly great attention [30, 37, 73]. Reconstructing hand-held objects from a single RGB image is a highly challenging and ill-posed problem. Suffering from the lack of real-world data and the ambiguity caused by hand- and self-occlusion, the performance of single-view hand-held object reconstruction remains limited.

Most existing works rely on Signed Distance Fields (SDFs) [37, 73] to represent the object shapes. Though effective under favorable conditions, such technique tends to result in over-smoothed and undetailed reconstructions [10, 51]. Moreover, prior works [30, 37, 73] typically utilize a deterministic modeling paradigm, which makes it hard to reason about the uncertainties introduced by hand- and self-occlusion. Recently, probabilistic point cloud denoising diffusion models [43, 44, 80] have shown to be effective for

*Authors with equal contributions.

the task of single-view object reconstruction. First, compared to works employing surface-based representations like SDFs, approaches reconstructing point clouds enjoy better capabilities in overcoming artifacts such as noise, sparsity, and irregularity [10]. Second, the probabilistic nature of denoising diffusion models is particularly beneficial for modeling uncertainty and indeterminacy. Therefore, in this work, we propose to leverage these probabilistic point cloud denoising diffusion models to conduct hand-held object reconstruction from a single RGB image.

Directly employing diffusion models in single-view hand-held object reconstruction, however, faces two main problems. **First**, diffusion models for 3D reconstruction typically assume isolated and unoccluded objects in the images [43, 44, 80] with self-occlusion properly modeled, while in hand-held object reconstruction tasks, hand occlusion needs to be modeled as well. In fact, the shape of the hand-held object is constrained by and highly related to the hand semantically and geometrically. **Second**, the object centroid is generally constrained by the hand vertices during the diffusion and the reverse processes. In existing diffusion models, the centroid of a partially denoised point cloud is not controlled and left variable, thus the centroid can easily deviate and move, for example, to the back side of the hand or even intersect with the hand, leading to physically implausible results. Additionally, the centroid bias causes the misalignment of the semantic features [19] and can thus have adverse effects on the object reconstruction quality.

To solve the aforementioned problems, we present HACD, a **Hand-Aware Conditional point cloud denoising Diffusion** probabilistic model for single-view hand-held object reconstruction (Fig. 1). To fully utilize the hand prior, we introduce hand-aware conditioning to model hand-object interaction from both semantic and geometric perspectives. Via extraction of local features from object and hand, we acquire a unified hand-object semantic embedding, which compensates for the semantic feature deficiency induced by the hand-occluded object region. Further, at each step, we explicitly encode the relative position between hand articulation and the partially denoised point cloud to obtain a geometric hand articulation embedding. To fuse the aforementioned semantic and geometric embeddings, we propose a novel dual-stream conditioning to separately predict noise features in two branches and then estimate the final noise from the integrated feature. Additionally, a hand-constrained centroid fixing scheme is proposed to ensure that the centroid of the partially denoised point cloud does not diverge during the diffusion as well as the reverse process. In particular, we use a small and efficient neural network to estimate the hand-constrained object centroid to properly guide the reverse diffusion. As a consequence, the model only needs to take care of the simpler shape diffusion, rather than having to simultaneously account for shape and centroid. Moreover,

leveraging the hand vertices constraint together with our centroid fixing can further enhance the precision and stability of our semantic and geometric features. Our contributions can be summarized as follows.

- We present HACD, a hand-aware conditional point cloud diffusion model for monocular hand-held object reconstruction, demonstrating superior performance in modeling the uncertainties induced by hand- and self-occlusion.
- We introduce a unified semantic hand-object embedding and a geometric hand articulation embedding to model semantic and geometric aspects of the shown hand-object interaction, which is subsequently utilized within our proposed dual-stream conditioning.
- We further propose a hand-constrained centroid fixing scheme, utilizing the hand vertices prior to prevent the centroid of the partially denoised point cloud from diverging during diffusion and its reverse processes.

Experiments on the synthetic ObMan [30] dataset and two real-world datasets, namely HO3D [29] and MOW [4], demonstrate that HACD can surpass all existing methods by a large margin.

2. Related Work

Hand Pose estimation. Hand pose estimation methods from RGB(-D) images can be primarily categorized into model-free and model-based methods. Model-free approaches typically detect 2D keypoints, which are then lifted to 3D joint positions [34, 47, 48, 50, 57, 58, 82], while model-based approaches exploit statistical models like MANO [59] with low-dimensional parameter spaces [1, 60, 63, 79, 81]. Compared with model-free methods, the model-based methods exhibit better robustness to occlusions and domain discrepancies. Therefore, our method utilizes an off-the-shelf model-based approach [60] to predict hand poses, which are then further utilized for shape inference of hand-held objects.

Single-view Object Reconstruction. Object reconstruction is a long-standing problem in the computer vision community. Traditionally, varieties of works focus on reconstruction from multiple-view geometric techniques [15, 16, 61, 76]. Recently, advanced by the powerful representation capacity of deep learning, single-view-based methods for object reconstruction have shown promising results [11, 44, 70, 71], in spite of the highly ill-posed setting. Early learning-based methods propose to learn category-specific networks [35, 36, 67], while more recent works try to learn a generalizable model across multiple categories for either meshes [26, 28], voxels [11, 25, 69], point clouds [22, 39], or implicit representations such as NeRFs [45] and SDFs [7, 51]. In this work, we focus on the difficult yet very important problem of learning hand-held object reconstruction from a single RGB image [30], putting a particular emphasis on modeling the impact of the hand occlusion.

Hand-Held Object Reconstruction. Reconstructing hand-held objects is very challenging due to intricate mutual occlusions and self-occlusions. Earlier works opt for the simplified task of 6DoF object pose estimation [17, 29, 31, 64, 66], assuming known object templates. To better utilize hand-object interactions, some studies reason about hand and object poses by means of implicit feature fusion [6, 40, 62, 66], exploiting explicit geometric constraints [2, 4, 12, 18, 27, 77, 78], or enforcing of physical constraints [52, 68]. Increasing attention has recently been paid to model-free hand-held object reconstruction, as it is a more applicable setting. Exemplarily, while [30] explicitly predicts the object mesh, [8, 9, 37] leverage implicit 3D representations such as signed distance functions for reconstructing the shape of the hand and object. However, all these methods follow a deterministic approach, oftentimes resulting in low-quality reconstruction results for occluded and invisible parts, especially in the ill-posed single-view setting. We instead draw inspiration from recent advances in probabilistic 3D generation [19, 33, 44, 80] and additionally leverage hand-articulation priors to achieve higher-fidelity hand-held object reconstruction.

Diffusion Models for 3D Reconstruction. Denoising diffusion models (DDMs) [33, 49] have recently attracted increasing attention in 3D reconstruction. While DMPGen [42] and LION [74] employ latent variables for the diffusion process in point cloud generation, PVD [80] directly applies DDMs to point clouds, leading to a unified framework for both unconditional 3D generation and conditional completion of partial shapes. Built on top of PVD, PC² [44] conducts single-view reconstruction by conditioning on projected image features. In this work, we employ point cloud diffusion models [44, 80] for our task of hand-held object reconstruction, as we found that these models are more robust towards producing fragmented or distorted surfaces under ambiguous views than existing SDF-based methods [73].

3. Method

Given a single-view RGB image I capturing a hand-held object, we aim at reconstructing the 3D point cloud of the object. As shown in Fig. 2, we first utilize an off-the-shelf method [30, 60] to predict hand parameters ϕ_H and camera view ϕ_C , where ϕ_H is defined using the MANO [59] hand model with 45DoF joint parameters and ϕ_C represents the 6DoF pose of the hand wrist in the world reference system. A hand-constrained centroid prediction network is then employed to predict the object centroid $\hat{\mathcal{M}}$ given the estimated hand vertices. Eventually, we use our centroid-fixed conditional point cloud diffusion model to reconstruct the object point cloud. Compared with existing diffusion models, our model can thus fully concentrate on the reconstruction of the shape, leading to an improved performance. We further leverage semantic as well as geometric hand

priors during diffusion. The unified semantic hand-object embedding and geometric hand articulation embedding are further used within our dual-stream conditioning. Due to the probabilistic nature of diffusion models together with our explicit modeling of hand-object interaction, HACD shows superior performance in handling uncertainties arising from hand- and self-occlusion.

In the following sections, we first introduce the fundamentals of conditional point cloud denoising diffusion models (Sec. 3.1). We then explain our novel hand-aware conditioning (Sec. 3.2), before describing our hand-constrained centroid-fixing scheme (Sec. 3.3).

3.1. Conditional Point Cloud Denoising Diffusion

We formulate single-view hand-held object reconstruction as conditional point cloud denoising diffusion, consisting of two Markov chains called the diffusion process and the reverse diffusion process. Suppose that we have a target point cloud with N points $X_0 \in \mathbb{R}^{3N}$ from the conditional distribution $q(X|z)$, where $z = I_{\phi_C, \phi_H}$ is the input RGB image capturing the hand-held object with the corresponding camera view ϕ_C and the hand pose ϕ_H . For the diffusion process, we gradually add Gaussian noise to the target point cloud at different levels $t \in \{1, \dots, T\}$ as

$$q(X_t|X_{t-1}, z) = \mathcal{N}(X_t|z; \sqrt{1 - \beta_t}X_{t-1}|z, \beta_t\mathbf{I}). \quad (1)$$

Notice that with a fixed variance schedule $\{\beta_t\}_{t=0}^T$, X_t can be simply expressed by X_0 according to

$$q(X_t|X_0, z) = \mathcal{N}(X_t|z; \sqrt{\bar{\alpha}_t}X_0|z, (1 - \bar{\alpha}_t)\mathbf{I}), \quad (2)$$

where $\alpha_t = 1 - \beta_t$, $\bar{\alpha}_t = \prod_{s=1}^t \alpha_s$. Therefore, we can reparameterize X_t as a linear combination of X_0 and a noise variable $\epsilon \sim \mathcal{N}(\mathbf{0}, \mathbf{I})$ as follows

$$X_t = \sqrt{\bar{\alpha}_t}X_0 + \sqrt{1 - \bar{\alpha}_t}\epsilon. \quad (3)$$

Starting with a point cloud sample X_T from random Gaussian noise, the reverse process iteratively samples from $q(X_{t-1}|X_t, z)$ to remove the added noise from the diffusion process. To approximate this reverse process, we train a conditional denoiser $\mathcal{D}_\theta(X_t, t, z)$ to learn the distribution $q(X_{t-1}|X_t, z)$ by

$$p_\theta(X_{t-1}|X_t, z) = \mathcal{N}(X_{t-1}; \mu_\theta(X_t, t, z), \sigma_t^2\mathbf{I}),$$

$$\mu_\theta(X_t, t, z) = \frac{1}{\sqrt{\alpha_t}}(X_t - \frac{1 - \alpha_t}{\sqrt{1 - \bar{\alpha}_t}}\epsilon_\theta(X_t, t, z)), \quad (4)$$

where μ_θ is the estimated mean.

3.2. Hand-Aware Conditioning

The essence of the conditional point cloud denoiser $\mathcal{D}_\theta(X_t, t, z)$ is the modeling of the condition z so to fully

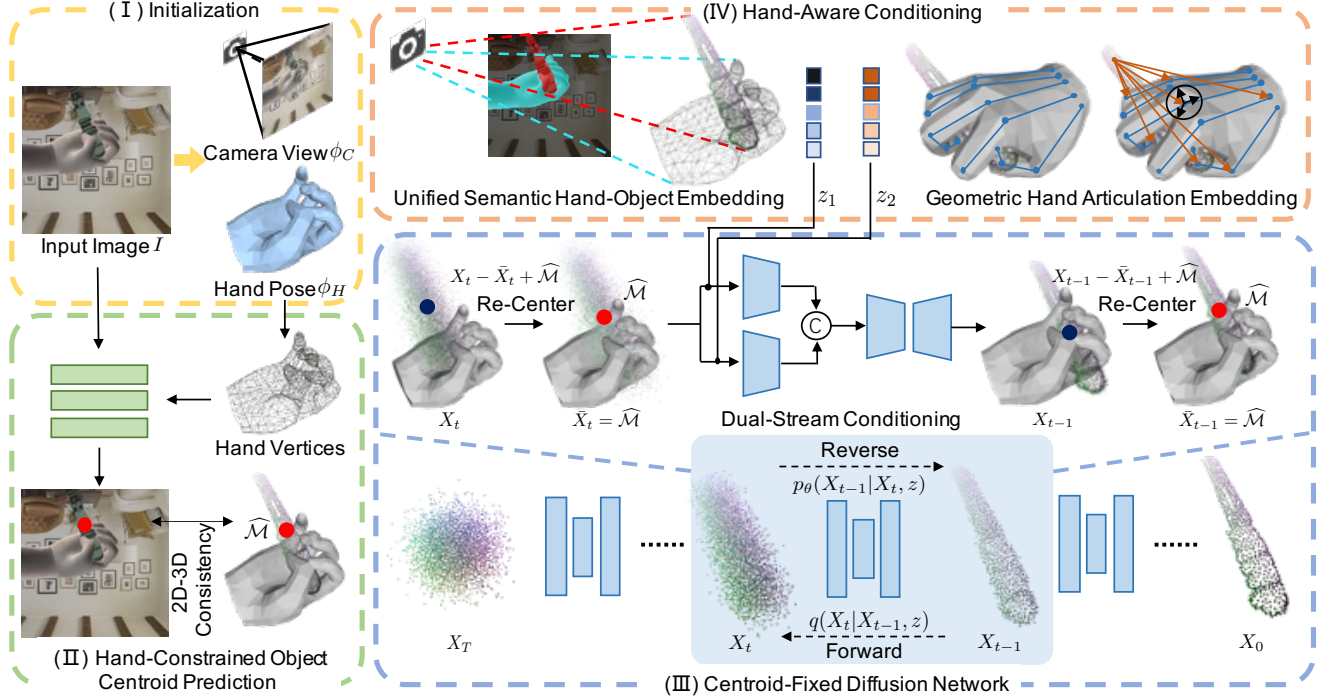


Figure 2. **Architecture of HACD.** (I) Given a single-view RGB image, we first predict the hand pose ϕ_H and camera view ϕ_C by an off-the-shelf network. (II) The object centroid $\hat{\mathcal{M}}$ is then estimated by our simple yet efficient hand-constrained centroid prediction network. (III) We further introduce a centroid-fixed diffusion network, which always keeps the centroid of partially denoised point cloud fixed at the predicted centroid $\hat{\mathcal{M}}$ during the reverse process. (IV) Both the unified semantic hand-object embedding and geometric hand articulation embedding are utilized as condition in the diffusion and the reverse process, which is then fused by a dual-stream conditioning scheme.

utilize the information of the input image along with the corresponding camera view and hand pose. Our key insight is that the hand can offer both semantic and geometric priors to facilitate object reconstruction. Therefore, a unified semantic hand-object embedding and a geometric hand articulation embedding are proposed in an effort to well model the hand-object interaction.

Unified Semantic Hand-Object Embedding. The 2D image feature is a vital component for object reconstruction. Unlike prior works that extract a global embedding for the image [11, 70, 71], we choose to compute unique semantic features for each point. Specifically, we first extract image features $\mathcal{F} \in \mathbb{R}^{H \times W \times C}$ by a standard 2D network such as ResNet [32] or ViT [21], with C being the number of feature channels. Instead of sharing the same global features among all points, we project the extracted image features onto the partially denoised point cloud at each diffusion step. Therefore, we design a corresponding projection function $\pi: \mathbb{R}^{H \times W \times C} \rightarrow \mathbb{R}^{N \times C}$, where N denotes the number of points in the point cloud. We implement π using the efficient point cloud rasterizer [56]. For every individual point within the point cloud, we obtain semantic features corresponding to the pixel onto which the point is rasterized. Subsequently, the pointwise semantic features at timestep t can be repre-

sented as $X_t^O = \pi(\mathcal{F}, \phi_C, X_t) \in \mathbb{R}^{N \times C}$.

However, due to the inevitable occlusion induced by the hand, it is very challenging to reconstruct the occluded part of the object as only a single view is provided. Due to the incomplete object semantic features, relying solely on the local features of object points alone is insufficient to conduct precise hand-held object reconstruction. On the other side, the hand information should not be fully ignored as the hand naturally contains information on the shape of the hand-occluded object region. Therefore, we apply π to both object and hand points to obtain $X_t^{HO} = \pi(\mathcal{F}, \phi_C, [X_t, P_H]) \in \mathbb{R}^{(N+N_H) \times C}$, which serves as a unified semantic hand-object embedding. Thereby, N_H denotes the number of the hand mesh vertices P_H , which can be obtained from the estimated hand pose ϕ_H together with the MANO hand model [59]. Noteworthy, we also apply an extra one-hot encoding to indicate whether the points belong to the object or the hand, hence making $X_t^{HO} \in \mathbb{R}^{(N+N_H) \times (C+1)}$.

Geometric Hand Articulation Embedding. Furthermore, the object shape is also highly constrained by the hand and very geometrically related to the hand articulation. In the core, the positions and directions of the hand joints in contact with the object, are supposed to be in accordance with the object surface for a stable hold. Therefore, knowing these

properties can serve as a strong prior to enhance reconstruction quality. In practice, we explicitly encode hand-object interaction by transforming the partially denoised point cloud at every step to each hand joint frame.

Given the partially denoised point cloud X_t and hand parameter ϕ_H , we first compute the rotation R_j and translation T_j of each joint j with respect to the hand wrist using forward kinematics given the hand model. We then transform X_t from the hand wrist coordinate system to each hand joint frame via $X_t^j = R_j X_t + T_j \in \mathbb{R}^{N \times 3}$ to encode the hand articulation onto object points. Finally, the hand articulation embedding $X_t^A \in \mathbb{R}^{N \times J}$ is calculated via concatenation and flattening of X_t^j , with J equaling 45 in our experiments as 15 hand joints are utilized.

Dual-Stream Conditioning. One possible approach is to directly concatenate the unified semantic hand-object embedding X_t^{HO} and geometric hand articulation embedding X_t^A as $z = [X_t^{HO}, X_t^A]$ and use it as condition. However, forcibly integrating semantic and geometric embeddings may lead to mutual interference. Instead, we propose a dual-stream conditioning strategy to fuse X_t^{HO} and X_t^A . In essence, we process $z_1 = X_t^{HO}$ and $z_2 = X_t^A$ separately through two distinct network branches, resulting in two features of identical dimensions, as shown in Fig. 2. The noise ϵ_θ is then predicted from the concatenated feature.

3.3. Hand-Constrained Centroid Fixing

Existing works commonly obtain the camera view ϕ_C and the hand pose ϕ_H using standard hand pose estimation methods [30, 60]. Without knowing the object pose during inference, we would need to denoise the points in the hand wrist coordinate system. However, directly using a diffusion model to simultaneously learn the object’s shape and pose is very difficult [19]. Thus, we propose a hand-constrained centroid fixing scheme to ease learning.

Centroid-Fixed Diffusion. We first reduce the problem of object pose estimation to centroid prediction, by defining a new object coordinate system. Essentially, while the origin of the object coordinate system is located at the centroid of the object, the axis orientation is shared with the hand wrist frame. Notice that during training, we can directly use the ground-truth object centroid \mathcal{M} to constrain the object point cloud. Therefore, we harness \mathcal{M} to stabilize the diffusion process and make the point cloud fixed at \mathcal{M} . In particular, during centroid-fixed diffusion, we re-center the object point cloud to \mathcal{M} and guarantee the added noise to be of zero-mean by

$$\begin{aligned} X_0 &\sim q(X_0), X_0 \leftarrow X_0 - \bar{X}_0 + \mathcal{M}, \\ \epsilon &\sim \mathcal{N}(\mathbf{0}, \mathbf{I}), \epsilon \leftarrow \epsilon - \bar{\epsilon}. \end{aligned} \quad (5)$$

Noteworthy, by keeping the object centroid unchanged, the misalignment error in semantic feature projection due to cen-

troid movements could also be alleviated. Thus, the training behavior becomes more stable as well.

Centroid Prediction for Reverse Diffusion. During the reverse diffusion process, we propose a simple yet effective hand-constrained network \mathcal{G} to predict the translation of the object w.r.t. the hand wrist coordinate system. Given the input RGB image I along with the corresponding hand pose ϕ_H and camera view ϕ_C , the predicted object centroid is obtained by

$$\widehat{\mathcal{M}} = \mathcal{G}(I_{\phi_C, \phi_H}). \quad (6)$$

As shown in Fig. 2 (II), \mathcal{G} first encodes the hand vertices P_H using PointNet [53] to constrain the object centroid in 3D space. Subsequently, the global hand features are combined with the image features extracted from a pre-trained ResNet-18 [32], followed by two parallel multilayer perceptrons (MLPs) to respectively output the 3D and 2D object centroids.

During the reverse process, we start from $X_T \sim \mathcal{N}(\mathbf{0}, \mathbf{I})$, $X_T \leftarrow X_T - \bar{X}_T + \widehat{\mathcal{M}}$. We then re-center the predicted noise and restrict the centroid of the denoised point cloud at $\widehat{\mathcal{M}}$ to remain consistent at each step $t \in \{T-1, \dots, 0\}$ according to

$$\begin{aligned} \epsilon_\theta &\leftarrow \epsilon_\theta - \bar{\epsilon}_\theta, \\ X_t &\sim p_\theta(X_t | X_{t+1}, z), X_t \leftarrow X_t - \bar{X}_t + \widehat{\mathcal{M}}. \end{aligned} \quad (7)$$

After the denoising process, we can directly obtain the reconstructed object point cloud by taking X_0 .

3.4. Training Objectives

We adopt Point-Voxel CNN (PVCNN) [41] for our diffusion model \mathcal{D}_θ , as it has demonstrated great results in 3D object reconstruction tasks [19, 44, 80]. The point cloud along with its corresponding condition $[X_t, X_t^Z] \in \mathbb{R}^{(3+C')N}$ is thereby fed into \mathcal{D}_θ to predict the noise $\epsilon_\theta \in \mathbb{R}^{3N}$, where C' denotes the number of hand-aware conditioning channels. Note that partial layers of PVCNN are adapted for dual-stream conditioning and the details are discussed in the supplementary material.

During optimization, we use the MSE loss between model output $\epsilon_\theta(X_t, t, z)$ and noise ϵ :

$$\mathcal{L}_{denoise} = \|\epsilon - \epsilon_\theta(X_t, t, z)\|, \epsilon \sim \mathcal{N}(\mathbf{0}, \mathbf{I}). \quad (8)$$

Notice that the centroid prediction network is separately trained from \mathcal{D}_θ . Thereby, the 3D object centroid \mathcal{M}_{3d} in the hand wrist frame and the 2D object centroid \mathcal{M}_{2d} in the normalized device coordinate (NDC) space are both supervised along with a 2D-3D projection loss. Overall, our total loss is defined as

$$\begin{aligned} \mathcal{L}_{centroid} &= \|\mathcal{M}_{3d} - \widehat{\mathcal{M}}_{3d}\| + \lambda_1 \|\mathcal{M}_{2d} - \widehat{\mathcal{M}}_{2d}\| \\ &\quad + \lambda_2 \|\mathcal{P}(\widehat{\mathcal{M}}_{3d}) - \widehat{\mathcal{M}}_{2d}\|, \end{aligned} \quad (9)$$

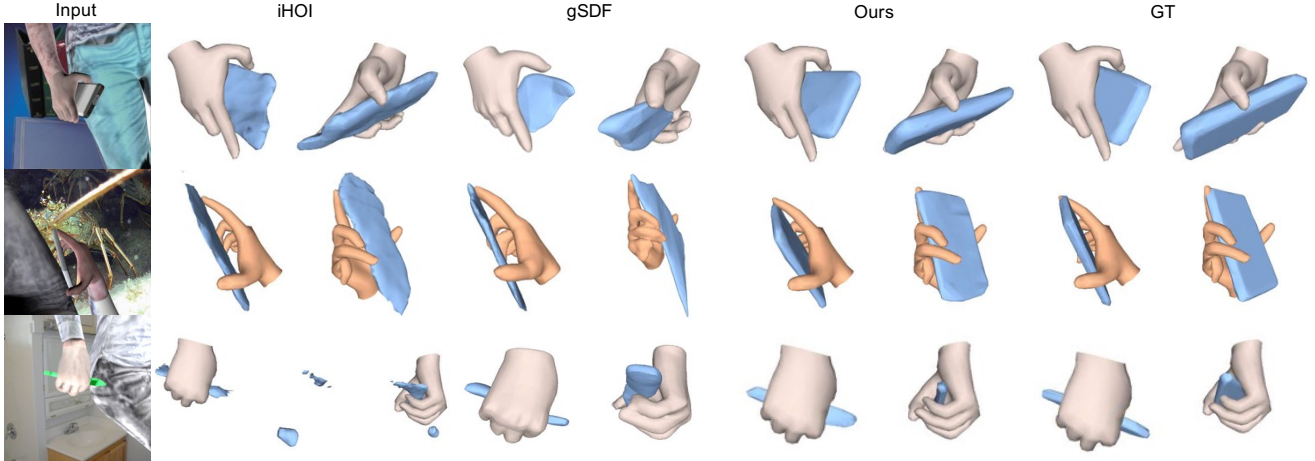


Figure 3. Qualitative results on the ObMan [30] dataset. For each method and ground truth, we show the reconstruction results in the camera view (column 1) and a novel view (column 2).

where λ_1 and λ_2 are hyperparameters, \mathcal{P} is the transformation from the hand wrist frame to the NDC space and $\hat{\cdot}$ refers to predicted results.

4. Experiments

4.1. Datasets and Setup

Datasets. We evaluate our method on three common benchmark datasets, including the synthetic ObMan [30] dataset and two real-world datasets, namely HO3D [29] and MOW [4]. **ObMan** [30] consists of 2,772 objects from 8 categories taken from ShapeNet [5], with 21K plausible grasps generated using GraspIt [46]. The dataset contains 141K frames for training and 6K frames for testing, which are rendered using Blender on top of random backgrounds. **HO3D** [29] includes 77,558 frames from 68 sequences, containing 10 different objects from the YCB dataset [3], which are manipulated by 10 different users. The hand and object pose annotations are obtained from multi-camera optimization procedures. **MOW** [4] consists of 442 images of 121 object templates, with in-the-wild source data collected from EPIC Kitchens [13, 14] and the 100 Days of Hands [62] datasets. We use the same training and testing split as iHOI [73]. Regarding hand pose prediction, we employ Hasson *et al.* [30] for the ObMan dataset and FrankMocap [60] for HO3D and MOW, in line with iHOI [73].

Evaluation Metrics. Following [73], we report the Chamfer Distance (CD) in mm and F-score at thresholds of 5mm (F-5) and 10mm (F-10) to compare with the state-of-the-art.

4.2. Evaluation on ObMan Dataset

We first present quantitative results on the large-scale synthetic ObMan dataset in Tab. 1. As can be seen, our approach surpasses all state-of-the-art methods by a large margin for

	F-5 \uparrow	F-10 \uparrow	CD \downarrow
HO [30]	0.23	0.56	0.64
GF [37]	0.30	0.51	1.39
AlignSDF [8]	0.40	0.64	-
iHOI [73]	0.42	0.63	1.02
gSDF [9]	0.44	0.66	-
Ours	0.56	0.75	0.27

Table 1. Comparison with State of the Arts on ObMan [30]. F-score of 5mm and 10mm, Chamfer Distance (mm) metrics are utilized for evaluation.

F-score and Chamfer Distance. Specifically, compared with the current best-performing method gSDF [9], we achieve a relative improvement of 27.3 % and 13.6 % for the F-5 and F-10 metrics, respectively. Furthermore, we can reduce the CD by 73.5 % compared with iHOI and 57.8 % compared with HO, demonstrating that our reconstructed shape possesses significantly fewer outliers.

We also visualize the reconstructed objects along with the hands in Fig. 3. While SDF-based methods, including iHOI [73] and gSDF [9], tend to result in either over-smoothed and less detailed, or fragmented reconstructions, our approach is able to generate geometrically coherent point clouds with plausible details, even for thin objects and heavily occluded parts.

4.3. Evaluation on Real-World Datasets

Aside from the synthetic ObMan dataset, we also conduct experiments on the two real-world datasets HO3D [29] and MOW [4] to demonstrate our approach’s generalization capabilities for real-world scenarios. The model is respectively finetuned on the two datasets, starting from the ObMan pre-trained model as initialization. As shown in Tab. 2 (top), our approach achieves state-of-the-art results on HO3D as

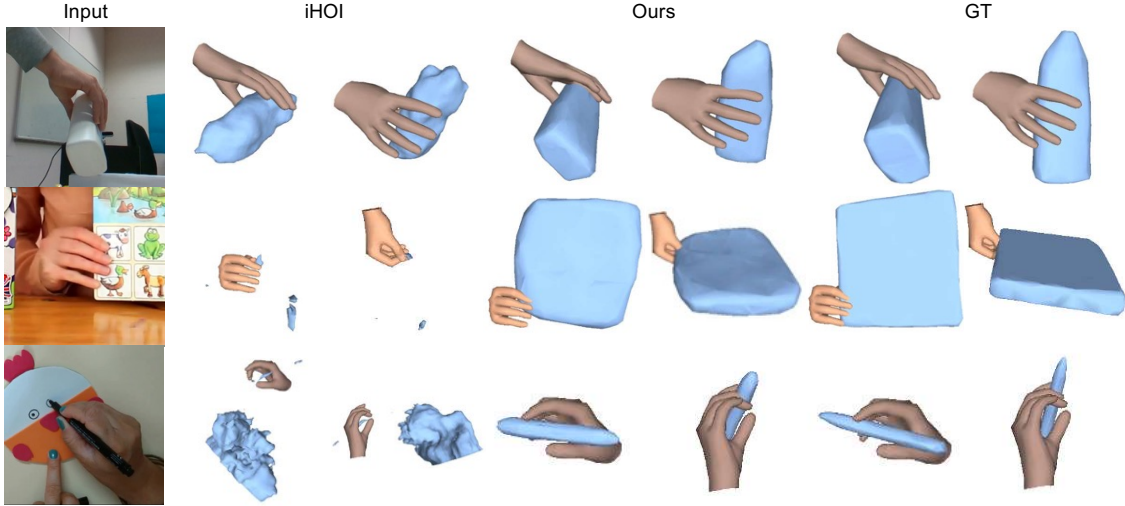


Figure 4. Qualitative results on HO3D [29] (top) and MOW [4] (middle and bottom) datasets. For each method and ground truth, we show the reconstruction results in the camera view (column 1) and a novel view (column 2).

	Finetuning	HO3D			MOW		
		F-5 \uparrow	F-10 \uparrow	CD \downarrow	F-5 \uparrow	F-10 \uparrow	CD \downarrow
HO [30]	✓	0.11	0.22	4.19	0.03	0.06	49.8
GF [37]	✓	0.12	0.24	4.96	0.06	0.13	40.1
iHOI [73]	✓	0.28	0.50	1.53	0.13	0.24	23.1
Ours	✓	0.36	0.55	0.66	0.25	0.39	1.86
iHOI [73]	✗	0.14	0.27	4.36	0.09*	0.17*	8.43*
Ours	✗	0.22	0.35	1.34	0.22	0.33	3.15

Table 2. Results on real-world datasets HO3D [29] and MOW [4]. We report results for both finetuning (top) and zero-shot transfer (bottom).

well as MOW. Concretely, regarding F-5 and F-10 metrics, we exhibit a noticeable average improvement of 19.3 % on the HO3D dataset and 77.4 % on the MOW dataset. Compared with the F-score metric, the Chamfer Distance metric is known to be more vulnerable to outliers [9, 65, 73]. Thus, the significant reduction of the CD metric illustrates that our approach is capable of producing significantly fewer outliers. The qualitative results in Fig. 4 also demonstrate the superiority of our approach.

Zero-shot transfer to HO3D and MOW. To further evaluate our zero-shot transfer abilities, we also directly apply our model, trained on the ObMan dataset, to HO3D and MOW without conducting any additional finetuning. The results in Tab. 2 (bottom) show that our method can again achieve a remarkable improvement on HO3D (57 % and 30 % in F-5 and F-10) and MOW (144 % and 94 % in F-5 and F-10), demonstrating the strength of HACD in synthetic-to-real generalization.

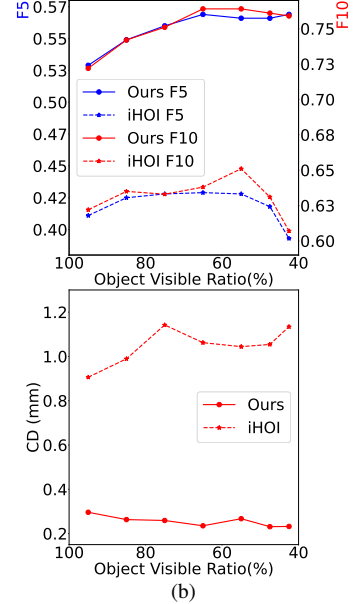
4.4. Ablation Studies

Effectiveness of hand-aware conditioning. In Tab. 3 (a), we show the impact of our proposed hand-aware conditioning. Both the hand semantic embedding (B2 vs. B0, A0 vs. B1) and the geometric hand articulation embedding (B1 vs. B0, A0 vs. B2) result in improved performance. Noteworthy, we can surpass existing methods on the ObMan dataset even without using any hand-aware conditioning (B0).

We further noticed that the way of encoding the hand-aware conditional information has a significant impact on performance. In particular, we have explored two alternative strategies to encode the hand-object interaction. First, inspired by [20], we implement a GCN-based hand embedding, which utilizes a graph convolutional network [23] for feature extraction. We again apply the GCN hand embedding to the partially denoised point cloud at each step. Although the GCN hand embedding implicitly encodes the hand articulation, it does not encode the hand-object interaction. Therefore, simply applying such an embedding as conditioning does not improve performance (See B3 vs. A0). Our hand articulation embedding, on the other hand, applies the unique articulation-aware embedding to each point of the partially denoised point cloud, which explicitly encodes hand-object interaction, thus significantly benefiting the object reconstruction performance. Second, we also utilize standard PointNet [53] to encode 3D hand vertices into a global hand embedding, which is then served to the partially denoised point cloud. Again, without modeling the hand-object interaction, the global hand embedding falls short of providing sufficient semantic information about the hand-occluded object. Consequently, the predictions end up being inferior to our proposed hand semantic embedding (B4 vs. A0).

Row	Method	ObMan			HO3D		
		F-5 \uparrow	F-10 \uparrow	CD \downarrow	F-5 \uparrow	F-10 \uparrow	CD \downarrow
A0	Ours	0.557	0.745	0.265	0.355	0.552	0.659
B0	A0 \rightarrow w/o hand-aware conditioning	0.478	0.667	0.407	0.279	0.461	0.964
B1	A0 \rightarrow w/o hand semantic embedding	0.510	0.694	0.373	0.325	0.496	0.809
B2	A0 \rightarrow w/o hand articulation embedding	0.510	0.693	0.383	0.301	0.483	0.885
B3	A0 \rightarrow w/ GCN hand embedding	0.523	0.713	0.297	0.338	0.537	0.522
B4	A0 \rightarrow w/ global hand embedding	0.524	0.711	0.301	0.309	0.490	0.859
B5	A0 \rightarrow w/o dual-stream conditioning	0.544	0.736	0.274	0.339	0.528	0.756
C0	B0 \rightarrow w/o centroid fixing	0.439	0.609	0.650	0.268	0.452	0.997
C1	B0 \rightarrow w/o centroid prediction	0.317	0.452	2.477	0.229	0.361	1.309
C2	C0 \rightarrow Test with GT object centroid	0.450	0.667	0.362	0.289	0.469	0.932
C3	C0 \rightarrow Test with GT object pose	0.499	0.703	0.343	0.307	0.485	0.841
D0	A0 \rightarrow Predicted hand pose + noise $\sigma = 0.1$	0.556	0.745	0.265	0.348	0.536	0.690
D1	A0 \rightarrow Predicted hand pose + noise $\sigma = 0.5$	0.517	0.707	0.319	0.321	0.504	0.837
E0	A0 \rightarrow GT hand pose	0.596	0.768	0.236	0.372	0.568	0.601
E1	A0 \rightarrow GT hand pose + noise $\sigma = 0.1$	0.572	0.761	0.262	0.358	0.556	0.642
E2	A0 \rightarrow GT hand pose + noise $\sigma = 0.5$	0.535	0.726	0.325	0.314	0.523	0.691
F0	C2 \rightarrow GT object centroid + noise $\sigma = 0.1$	0.442	0.647	0.341	0.281	0.459	1.002
F1	C2 \rightarrow GT object centroid + noise $\sigma = 0.5$	0.411	0.601	0.495	0.236	0.422	1.228

(a)



(b)

Table 3. **Ablation study.** (a) Ablation on ObMan [30] and HO3D [29] datasets. (b) Robustness against hand occlusion. We analyze the patterns of the F-5, F-10, and CD metrics as a function of the object visibility ratio on the test set of ObMan [30].

Effectiveness of dual-stream conditioning. Instead of integrating our unified semantic hand-object and geometric hand articulation embeddings by the proposed dual-stream architecture, we simply concatenate the embeddings. Note that we concatenate a zero matrix to the hand articulation embedding to meet the dimension of unified semantic hand-object embedding. The declined results (B5 vs. A0) demonstrate that dual-stream conditioning enhances reconstruction performance by independently processing semantic and geometric embeddings, ensuring their mutual independence.

Effectiveness of hand-constrained centroid fixing. In Tab. 3 (a), we illustrate the importance of the centroid fixing scheme. Our centroid fixing operation improves the precision and robustness of the semantic and geometric embedding, thus enhancing the performance (B0 vs. C0). Further, without the hand-constrained centroid prediction network, the diffusion model has to simultaneously learn the centroid deviation and object shape, which leads to clearly worse results (C1 vs. B0). Additionally, in C2 we report results when using the actual ground-truth object centroid and in C3 when using the ground-truth object pose. Without our centroid fixing scheme, the results remain non-comparable even when testing with the ground-truth object centroid (C2 vs. B0). This further demonstrates the effectiveness of our proposed centroid fixing scheme.

Robustness against hand pose prediction quality. To demonstrate that our method is able to deal with noisy hand pose estimates, we add various levels of Gaussian noise to predicted hand poses. Notice that adding $\sigma = 0.1$ noise has almost no effect on the performance (D0 vs. A0) for both

ObMan and HO3D. Further, despite a slight decrease in performance with $\sigma = 0.5$ noise (D1 vs. A0), the results clearly show that our approach is robust towards weak hand pose predictions. Additionally, in E0 we explore the upper bound of our method using ground-truth hand poses, and in E1 / E2 we further demonstrate the robustness against noisy hand pose prediction.

Robustness against object centroid prediction quality. We also add different levels of Gaussian noise to the ground-truth object centroid (F0 / F1) to constitute the robustness of our method towards inaccurate object centroid.

Robustness against hand occlusion. To illustrate the robustness of our approach against hand occlusion, we split the test set of ObMan into groups according to the visible ratio of the object and compute the mean F-score and CD for each group. As shown in Tab. 3 (b), when the object is undergoing strong occlusion by the hand (object visible ratio $< 50\%$), iHOI suffers a significant decline in both F-5 and F-10 metrics, while the performance of our approach remains steady. The quantitative results of CD metric also demonstrate that aided by our proposed hand-aware conditioning and hand-constrained centroid fixing scheme, HACD is capable of modeling the uncertainties induced by hand occlusion.

5. Conclusion

In this paper, we present HACD, a novel hand-aware point cloud diffusion model for single-view hand-held object reconstruction. HACD does not require any object templates, category priors, or depth information, and exhibits supe-

rior performance in modeling the uncertainties induced by hand- and self-occlusion. In the core, we introduce hand-aware conditioning to model the semantic and geometric aspects of hand-object interactions. We further propose a hand-constrained centroid-fixing scheme, utilizing the estimated hand vertices to prevent the centroid of the partially denoised point cloud from diverging during diffusion and reverse processes. The experiments on ObMan, HO3D, and MOW datasets demonstrate that our approach surpasses existing methods in both synthetic and real-world scenarios.

References

- [1] Adnane Boukhayma, Rodrigo de Bem, and Philip HS Torr. 3d hand shape and pose from images in the wild. In *CVPR*, pages 10843–10852, 2019. 2
- [2] Samarth Brahmabhatt, Chengcheng Tang, Christopher D Twigg, Charles C Kemp, and James Hays. Contactpose: A dataset of grasps with object contact and hand pose. In *ECCV*, pages 361–378. Springer, 2020. 3
- [3] Berk Calli, Arjun Singh, Aaron Walsman, Siddhartha Srinivasa, Pieter Abbeel, and Aaron M Dollar. The ycb object and model set: Towards common benchmarks for manipulation research. In *2015 international conference on advanced robotics (ICAR)*, pages 510–517. IEEE, 2015. 6
- [4] Zhe Cao, Ilija Radosavovic, Angjoo Kanazawa, and Jitendra Malik. Reconstructing hand-object interactions in the wild. In *ICCV*, pages 12417–12426, 2021. 1, 2, 3, 6, 7
- [5] Angel X Chang, Thomas Funkhouser, Leonidas Guibas, Pat Hanrahan, Qixing Huang, Zimo Li, Silvio Savarese, Manolis Savva, Shuran Song, Hao Su, et al. Shapenet: An information-rich 3d model repository. *arXiv preprint arXiv:1512.03012*, 2015. 6
- [6] Yujin Chen, Zhigang Tu, Di Kang, Ruizhi Chen, Linchao Bao, Zhengyou Zhang, and Junsong Yuan. Joint hand-object 3d reconstruction from a single image with cross-branch feature fusion. *IEEE TIP*, 30:4008–4021, 2021. 3
- [7] Zhiqin Chen and Hao Zhang. Learning implicit fields for generative shape modeling. In *CVPR*, pages 5939–5948, 2019. 2
- [8] Zerui Chen, Yana Hasson, Cordelia Schmid, and Ivan Laptev. Alignsdf: Pose-aligned signed distance fields for hand-object reconstruction. In *ECCV*, pages 231–248. Springer, 2022. 3, 6
- [9] Zerui Chen, Shizhe Chen, Cordelia Schmid, and Ivan Laptev. gsdf: Geometry-driven signed distance functions for 3d hand-object reconstruction. In *CVPR*, pages 12890–12900, 2023. 3, 6, 7
- [10] Jaesung Choe, ByeongIn Joung, Francois Rameau, Jaesik Park, and In So Kweon. Deep point cloud reconstruction. In *ICLR*, 2021. 1, 2
- [11] Christopher B Choy, Danfei Xu, JunYoung Gwak, Kevin Chen, and Silvio Savarese. 3d-r2n2: A unified approach for single and multi-view 3d object reconstruction. In *ECCV*, pages 628–644. Springer, 2016. 2, 4
- [12] Enric Corona, Albert Pumarola, Guillem Alenya, Francesc Moreno-Noguer, and Grégory Rogez. Ganhand: Predicting human grasp affordances in multi-object scenes. In *CVPR*, pages 5031–5041, 2020. 3
- [13] Dima Damen, Hazel Doughty, Giovanni Maria Farinella, Sanja Fidler, Antonino Furnari, Evangelos Kazakos, Davide Moltisanti, Jonathan Munro, Toby Perrett, Will Price, et al. Scaling egocentric vision: The epic-kitchens dataset. In *ECCV*, pages 720–736, 2018. 6
- [14] Dima Damen, Hazel Doughty, Giovanni Maria Farinella, Sanja Fidler, Antonino Furnari, Evangelos Kazakos, Davide Moltisanti, Jonathan Munro, Toby Perrett, Will Price, and Michael Wray. The epic-kitchens dataset: Collection, challenges and baselines. *IEEE TPAMI*, 43(11):4125–4141, 2021. 6
- [15] Yan Di, Henrique Morimitsu, Shan Gao, and Xiangyang Ji. Monocular piecewise depth estimation in dynamic scenes by exploiting superpixel relations. In *Proceedings of the IEEE/CVF International Conference on Computer Vision*, pages 4363–4372, 2019. 2
- [16] Yan Di, Henrique Morimitsu, Zhiqiang Lou, and Xiangyang Ji. A unified framework for piecewise semantic reconstruction in dynamic scenes via exploiting superpixel relations. In *2020 IEEE International Conference on Robotics and Automation (ICRA)*, pages 10737–10743. IEEE, 2020. 2
- [17] Yan Di, Fabian Manhardt, Gu Wang, Xiangyang Ji, Nassir Navab, and Federico Tombari. So-pose: Exploiting self-occlusion for direct 6d pose estimation. In *Proceedings of the IEEE/CVF International Conference on Computer Vision*, pages 12396–12405, 2021. 3
- [18] Yan Di, Ruida Zhang, Zhiqiang Lou, Fabian Manhardt, Xiangyang Ji, Nassir Navab, and Federico Tombari. Gpv-pose: Category-level object pose estimation via geometry-guided point-wise voting. In *Proceedings of the IEEE/CVF Conference on Computer Vision and Pattern Recognition*, pages 6781–6791, 2022. 3
- [19] Yan Di, Chenyangguang Zhang, Pengyuan Wang, Guangyao Zhai, Ruida Zhang, Fabian Manhardt, Benjamin Busam, Xiangyang Ji, and Federico Tombari. Ccd-3dr: Consistent conditioning in diffusion for single-image 3d reconstruction. *arXiv preprint arXiv:2308.07837*, 2023. 2, 3, 5
- [20] Bardia Doosti, Shujon Naha, Majid Mirbagheri, and David J Crandall. Hope-net: A graph-based model for hand-object pose estimation. In *CVPR*, pages 6608–6617, 2020. 7
- [21] Alexey Dosovitskiy, Lucas Beyer, Alexander Kolesnikov, Dirk Weissenborn, Xiaohua Zhai, Thomas Unterthiner, Mostafa Dehghani, Matthias Minderer, Georg Heigold, Sylvain Gelly, Jakob Uszkoreit, and Neil Houlsby. An image is worth 16x16 words: Transformers for image recognition at scale. *ICLR*, 2021. 4
- [22] Haoqiang Fan, Hao Su, and Leonidas J Guibas. A point set generation network for 3d object reconstruction from a single image. In *CVPR*, pages 605–613, 2017. 2
- [23] Hongyang Gao and Shuiwang Ji. Graph u-nets. In *ICML*, pages 2083–2092. PMLR, 2019. 7
- [24] Qing Gao, Yongquan Chen, Zhaojie Ju, and Yi Liang. Dynamic hand gesture recognition based on 3d hand pose estimation for human-robot interaction. *IEEE Sensors Journal*, 22(18):17421–17430, 2021. 1

- [25] Rohit Girdhar, David F Fouhey, Mikel Rodriguez, and Abhinav Gupta. Learning a predictable and generative vector representation for objects. In *ECCV*, pages 484–499. Springer, 2016. 2
- [26] Georgia Gkioxari, Jitendra Malik, and Justin Johnson. Mesh r-cnn. In *ICCV*, pages 9785–9795, 2019. 2
- [27] Patrick Grady, Chengcheng Tang, Christopher D Twigg, Minh Vo, Samarth Brahmabhatt, and Charles C Kemp. Contactopt: Optimizing contact to improve grasps. In *CVPR*, pages 1471–1481, 2021. 3
- [28] Thibault Groueix, Matthew Fisher, Vladimir G Kim, Bryan C Russell, and Mathieu Aubry. A papier-mâché approach to learning 3d surface generation. In *CVPR*, pages 216–224, 2018. 2
- [29] Shreyas Hampali, Mahdi Rad, Markus Oberweger, and Vincent Lepetit. Honnotate: A method for 3d annotation of hand and object poses. In *CVPR*, pages 3196–3206, 2020. 2, 3, 6, 7, 8
- [30] Yana Hasson, Gul Varol, Dimitrios Tzionas, Igor Kalevatykh, Michael J Black, Ivan Laptev, and Cordelia Schmid. Learning joint reconstruction of hands and manipulated objects. In *CVPR*, pages 11807–11816, 2019. 1, 2, 3, 5, 6, 7, 8
- [31] Yana Hasson, Bugra Tekin, Federica Bogo, Ivan Laptev, Marc Pollefeys, and Cordelia Schmid. Leveraging photometric consistency over time for sparsely supervised hand-object reconstruction. In *CVPR*, pages 571–580, 2020. 3
- [32] Kaiming He, Xiangyu Zhang, Shaoqing Ren, and Jian Sun. Deep residual learning for image recognition. In *CVPR*, pages 770–778, 2016. 4, 5
- [33] Jonathan Ho, Ajay Jain, and Pieter Abbeel. Denoising diffusion probabilistic models. *NeurIPS*, 33:6840–6851, 2020. 3
- [34] Umar Iqbal, Pavlo Molchanov, Thomas Breuel Juergen Gall, and Jan Kautz. Hand pose estimation via latent 2.5 d heatmap regression. In *ECCV*, pages 118–134, 2018. 2
- [35] Angjoo Kanazawa, Shubham Tulsiani, Alexei A Efros, and Jitendra Malik. Learning category-specific mesh reconstruction from image collections. In *ECCV*, pages 371–386, 2018. 2
- [36] Abhishek Kar, Shubham Tulsiani, Joao Carreira, and Jitendra Malik. Category-specific object reconstruction from a single image. In *CVPR*, pages 1966–1974, 2015. 2
- [37] Korrawe Karunratanakul, Jinlong Yang, Yan Zhang, Michael J Black, Krikamol Muandet, and Siyu Tang. Grasping field: Learning implicit representations for human grasps. In *3DV*, pages 333–344. IEEE, 2020. 1, 3, 6, 7
- [38] Zhiying Leng, Jiaying Chen, Hubert PH Shum, Frederick WB Li, and Xiaohui Liang. Stable hand pose estimation under tremor via graph neural network. In *2021 IEEE Virtual Reality and 3D User Interfaces (VR)*, pages 226–234. IEEE, 2021. 1
- [39] Chen-Hsuan Lin, Chen Kong, and Simon Lucey. Learning efficient point cloud generation for dense 3d object reconstruction. In *AAAI*, 2018. 2
- [40] Shaowei Liu, Hanwen Jiang, Jiarui Xu, Sifei Liu, and Xiaolong Wang. Semi-supervised 3d hand-object poses estimation with interactions in time. In *CVPR*, pages 14687–14697, 2021. 3
- [41] Zhijian Liu, Haotian Tang, Yujun Lin, and Song Han. Point-voxel cnn for efficient 3d deep learning. *NeurIPS*, 32, 2019. 5
- [42] Shitong Luo and Wei Hu. Diffusion probabilistic models for 3d point cloud generation. In *CVPR*, pages 2837–2845, 2021. 3
- [43] Shitong Luo and Wei Hu. Diffusion probabilistic models for 3d point cloud generation. In *CVPR*, pages 2837–2845, 2021. 1, 2
- [44] Luke Melas-Kyriazi, Christian Rupprecht, and Andrea Vedaldi. PC²: Projection-conditioned point cloud diffusion for single-image 3D reconstruction. In *CVPR*, pages 12923–12932, 2023. 1, 2, 3, 5
- [45] Ben Mildenhall, Pratul P. Srinivasan, Matthew Tancik, Jonathan T. Barron, Ravi Ramamoorthi, and Ren Ng. Nerf: Representing scenes as neural radiance fields for view synthesis. In *ECCV*, 2020. 2
- [46] Andrew T Miller and Peter K Allen. Graspit! a versatile simulator for robotic grasping. *IEEE Robotics & Automation Magazine*, 11(4):110–122, 2004. 6
- [47] Franziska Mueller, Florian Bernard, Oleksandr Sotnychenko, Dushyant Mehta, Srinath Sridhar, Dan Casas, and Christian Theobalt. Gnerated hands for real-time 3d hand tracking from monocular rgb. In *CVPR*, pages 49–59, 2018. 2
- [48] Franziska Mueller, Micah Davis, Florian Bernard, Oleksandr Sotnychenko, Mickeal Verschoor, Miguel A Otaduy, Dan Casas, and Christian Theobalt. Real-time pose and shape reconstruction of two interacting hands with a single depth camera. *ACM TOG*, 38(4):1–13, 2019. 2
- [49] Alexander Quinn Nichol and Prafulla Dhariwal. Improved denoising diffusion probabilistic models. In *ICML*, pages 8162–8171. PMLR, 2021. 3
- [50] Paschalis Panteleris, Iason Oikonomidis, and Antonis Argyros. Using a single rgb frame for real time 3d hand pose estimation in the wild. In *WACV*, pages 436–445. IEEE, 2018. 2
- [51] Jeong Joon Park, Peter Florence, Julian Straub, Richard Newcombe, and Steven Lovegrove. DeepSDF: Learning continuous signed distance functions for shape representation. In *CVPR*, pages 165–174, 2019. 1, 2
- [52] Tu-Hoa Pham, Nikolaos Kyriazis, Antonis A Argyros, and Abderrahmane Kheddar. Hand-object contact force estimation from markerless visual tracking. *IEEE TPAMI*, 40(12):2883–2896, 2017. 3
- [53] Charles R Qi, Hao Su, Kaichun Mo, and Leonidas J Guibas. Pointnet: Deep learning on point sets for 3d classification and segmentation. In *CVPR*, pages 652–660, 2017. 5, 7
- [54] Xun Qian, Fengming He, Xiyun Hu, Tianyi Wang, and Karthik Ramani. Arnnotate: An augmented reality interface for collecting custom dataset of 3d hand-object interaction pose estimation. In *Proceedings of the 35th Annual ACM Symposium on User Interface Software and Technology*, pages 1–14, 2022. 1
- [55] Hanna-Riikka Rantamaa, Jari Kangas, Sriram Kishore Kumar, Helena Mehtonen, Jorma Järnstedt, and Roope Raisamo. Comparison of a vr stylus with a controller, hand tracking, and a mouse for object manipulation and medical marking tasks in virtual reality. *Applied Sciences*, 13(4):2251, 2023. 1

- [56] Nikhila Ravi, Jeremy Reizenstein, David Novotny, Taylor Gordon, Wan-Yen Lo, Justin Johnson, and Georgia Gkioxari. Accelerating 3d deep learning with pytorch3d. *arXiv preprint arXiv:2007.08501*, 2020. 4
- [57] Grégory Rogez, Maryam Khademi, JS Supančič III, Jose Maria Martinez Montiel, and Deva Ramanan. 3d hand pose detection in egocentric rgb-d images. In *ECCVW*, pages 356–371. Springer, 2015. 2
- [58] Grégory Rogez, James S Supancic, and Deva Ramanan. Understanding everyday hands in action from rgb-d images. In *ICCV*, pages 3889–3897, 2015. 2
- [59] Javier Romero, Dimitrios Tzionas, and Michael J. Black. Embodied hands: Modeling and capturing hands and bodies together. *ACM TOG*, 36(6), 2017. 2, 3, 4
- [60] Yu Rong, Takaaki Shiratori, and Hanbyul Joo. Frankmocap: A monocular 3d whole-body pose estimation system via regression and integration. In *ICCVW*, 2021. 2, 3, 5, 6
- [61] Johannes Lutz Schönberger and Jan-Michael Frahm. Structure-from-motion revisited. In *CVPR*, 2016. 2
- [62] Dandan Shan, Jiaqi Geng, Michelle Shu, and David F Fouhey. Understanding human hands in contact at internet scale. In *CVPR*, pages 9869–9878, 2020. 3, 6
- [63] Srinath Sridhar, Franziska Mueller, Antti Oulasvirta, and Christian Theobalt. Fast and robust hand tracking using detection-guided optimization. In *CVPR*, pages 3213–3221, 2015. 2
- [64] Srinath Sridhar, Franziska Mueller, Michael Zollhöfer, Dan Casas, Antti Oulasvirta, and Christian Theobalt. Real-time joint tracking of a hand manipulating an object from rgb-d input. In *ECCV*, pages 294–310. Springer, 2016. 3
- [65] Maxim Tatarchenko, Stephan R Richter, René Ranftl, Zhuwen Li, Vladlen Koltun, and Thomas Brox. What do single-view 3d reconstruction networks learn? In *CVPR*, pages 3405–3414, 2019. 7
- [66] Bugra Tekin, Federica Bogo, and Marc Pollefeys. H+o: Unified egocentric recognition of 3d hand-object poses and interactions. In *CVPR*, 2019. 3
- [67] Shubham Tulsiani, Abhishek Kar, Joao Carreira, and Jitendra Malik. Learning category-specific deformable 3d models for object reconstruction. *IEEE TPAMI*, 39(4):719–731, 2016. 2
- [68] Dimitrios Tzionas, Luca Ballan, Abhilash Srikantha, Pablo Aponte, Marc Pollefeys, and Juergen Gall. Capturing hands in action using discriminative salient points and physics simulation. *IJCV*, 118:172–193, 2016. 3
- [69] Jiajun Wu, Chengkai Zhang, Tianfan Xue, Bill Freeman, and Josh Tenenbaum. Learning a probabilistic latent space of object shapes via 3d generative-adversarial modeling. *NeurIPS*, 29, 2016. 2
- [70] Haozhe Xie, Hongxun Yao, Xiaoshuai Sun, Shangchen Zhou, and Shengping Zhang. Pix2vox: Context-aware 3d reconstruction from single and multi-view images. In *ICCV*, pages 2690–2698, 2019. 2, 4
- [71] Haozhe Xie, Hongxun Yao, Shengping Zhang, Shangchen Zhou, and Wenxiu Sun. Pix2vox++: Multi-scale context-aware 3d object reconstruction from single and multiple images. *IJCV*, 128(12):2919–2935, 2020. 2, 4
- [72] Lixin Yang, Xinyu Zhan, Kailin Li, Wenqiang Xu, Jiefeng Li, and Cewu Lu. Cpf: Learning a contact potential field to model the hand-object interaction. In *ICCV*, pages 11097–11106, 2021. 1
- [73] Yufei Ye, Abhinav Gupta, and Shubham Tulsiani. What’s in your hands? 3D reconstruction of generic objects in hands. In *CVPR*, pages 3895–3905, 2022. 1, 3, 6, 7
- [74] Xiaohui Zeng, Arash Vahdat, Francis Williams, Zan Gojcic, Or Litany, Sanja Fidler, and Karsten Kreis. Lion: Latent point diffusion models for 3d shape generation. In *NeurIPS*, 2022. 3
- [75] Guangyao Zhai, Xiaoni Cai, Dianye Huang, Yan Di, Fabian Manhardt, Federico Tombari, Nassir Navab, and Benjamin Busam. Sg-bot: Object rearrangement via coarse-to-fine robotic imagination on scene graphs. *arXiv preprint arXiv:2309.12188*, 2023. 1
- [76] Chenyangguang Zhang, Zhiqiang Lou, Yan Di, Federico Tombari, and Xiangyang Ji. Sst: Real-time end-to-end monocular 3d reconstruction via sparse spatial-temporal guidance. In *2023 IEEE International Conference on Multimedia and Expo (ICME)*, pages 2033–2038. IEEE, 2023. 2
- [77] Ruida Zhang, Yan Di, Zhiqiang Lou, Fabian Manhardt, Federico Tombari, and Xiangyang Ji. Rbp-pose: Residual bounding box projection for category-level pose estimation. In *European Conference on Computer Vision*, pages 655–672. Springer, 2022. 3
- [78] Ruida Zhang, Yan Di, Fabian Manhardt, Federico Tombari, and Xiangyang Ji. Ssp-pose: Symmetry-aware shape prior deformation for direct category-level object pose estimation. In *2022 IEEE/RSJ International Conference on Intelligent Robots and Systems (IROS)*, pages 7452–7459. IEEE, 2022. 3
- [79] Xiong Zhang, Qiang Li, Hong Mo, Wenbo Zhang, and Wen Zheng. End-to-end hand mesh recovery from a monocular rgb image. In *ICCV*, pages 2354–2364, 2019. 2
- [80] Linqi Zhou, Yilun Du, and Jiajun Wu. 3d shape generation and completion through point-voxel diffusion. In *ICCV*, pages 5826–5835, 2021. 1, 2, 3, 5
- [81] Yuxiao Zhou, Marc Habermann, Weipeng Xu, Ikhsanul Habbie, Christian Theobalt, and Feng Xu. Monocular real-time hand shape and motion capture using multi-modal data. In *CVPR*, pages 5346–5355, 2020. 2
- [82] Christian Zimmermann and Thomas Brox. Learning to estimate 3d hand pose from single rgb images. In *ICCV*, pages 4903–4911, 2017. 2